Evaluation of Left Ventricle Myocardium Detection by a Fully Automatic Segmentation Using Geodesic Active Contour

Gustavo Canavaci Barizon, Antonio Carlos da Silva Senra Filho, André Schmidt, and Luiz Otávio Murta Junior

Abstract

Cardiac MRI has experienced a crescent relevance in clinical investigations. The segmentation of myocardial walls is a prerequisite for assessment of cardiac viability. Manual or semi-automatic segmentation of all the images of a subject is tedious, as well as consuming much time from cardiologists. In this study, we selected 23 slices of simulated cardiac MR by MRXCAT and 30 real slices of CINE-MR from 15 patients with Chagas Disease. The proposed pipeline of the fully automatic segmentation consists of three steps: 1. Preprocessing; 2. Automatic Seeds Definition; and 3. Segmentation by Geodesic Active Contour. An experienced cardiologist provided the gold standard annotations of apical, mid-ventricular and basal LV myocardium. We use the following three metrics to validate the proposed pipeline with different signal to noise ratio: Dice similarity (DS), Precision (Pr) and Volumetric Similarity (VS). DS show good agreement between manual segmentation and the automatic segmentation in simulated images with SNR 200, 25, 15 and 5, i.e., 0.98, 0.93, 0.9 and 0.72, respectively. We found moderate agreements between manual segmentation and Snake segmentation in simulated images with SNR 200, 25, 15 and 5, i.e., 0.38, 0.42, 0.34 and 0.39, respectively. The DS, VS, and Pr obtained suggest substantial agreements between the manual and our proposed method segmentation in images of Chagas's Disease, i.e., 0.8 [0.69–0.87], 0.89 [0.72–0.99] and 0.9 [0.76–0.98] (mean [min–max]), respectively. Our findings suggest that one can use the proposed method in the automatic myocardium segmentation with reliability similar to manual tracing, although completely free of human interaction.

1 Introduction

Cardiovascular diseases are the leading cause of death in the world. The cardiovascular magnetic resonance (CMR) imaging is the best technique is ionizing radiation free and can provide a good and clear structural anatomy of the heart [1]. Cardiac cine-MRI is considered the standard MR technique mainly used for global function measurements and can achieve high-resolution images concerning the cardiac borders.

Segmentation consists in dividing an image or object into multiple segments, extracting regions of interest. The segmentation of myocardial walls is a prerequisite for assessment of cardiac viability and development of clinical applications. Manual segmentation of all the images of a subject is tedious, as well as consuming much time from cardiologists [2]. Epicardial delineation is more difficult than endocardial delineation due to the similarity of the gray level of the outer tissues and the heart and poor contrast. However, endocardial delineation is more accessible due to the high contrast between the blood and the myocardium in all the modalities [1]. Usually, apical slices are more difficult to the segment in all the modalities due to less information, unpredictable end of the left ventricle (LV) and right ventricle (RV) cavities, vicinity of the diaphragm and more variable shape. Basal slices are also more cumbersome to segment due to highly variable shape and motion of the LV and RV walls.

G. C. Barizon (✉) · A. C. da Silva Senra Filho · L. O. M. Junior
Department of Computing and Mathematics, University of São Paulo, Ribeirão Preto, Brazil
e-mail: gustavo.canavaci@usp.br

A. Schmidt
Division of Cardiology, Medical School of Ribeirão Preto, University of São Paulo, Ribeirão Preto, Brazil

In the last few years, numerous methods were developed for segmenting the cardiac ventricle. Recent studies [3–11] have shown the importance of automatic segmentation methods to assess of cardiac function. The automatic segmentation algorithms provide a better assessment of volumes, ejection fraction, and thickening analysis. Thus, the challenges in segmenting myocardium in cardiac MR are multiple. In this article, we present a workflow for fully automatic LV myocardial segmentation in cardiac MR.

2 Methods

In our study, we selected 23 consecutive slices of simulated cardiac MR image by MRXCAT. The MRXCAT is a simulation framework that allows for realistic simulation of CMR including optional cardiac and respiratory motion [12]. Also, we selected representative apical, mid-ventricular and basal CINE-MR slices from 15 patients with Chagas's Disease. All images were acquired, anonymized and stored in DICOM format, by ethical standards.

CINE MRI was performed using a 1.5 T magnetic resonance scanner (Philips Achieva) at the University Hospital of the Ribeirão Preto Medical School, University of São Paulo. MRI imaging parameters were: resolution 0.8 pixels per mm, pixel size 1.25 × 1.25, image matrix 256 × 256, flip angle 60°, slice thickness 8 mm with 10 mm spacing between slices.

The Research Ethics Committee of the São Paulo University Hospital approved the study. We conducted the study in accordance with the precepts of the Declaration of Helsinki. All patients gave written informed consent to participate.

2.1 Processing and Analysis

We processed the acquired images using an extension developed in our laboratory, i.e., 3D Slicer, Insight Toolkit (ITK) and Visualization Toolkit (VTK) [13, 14]. The proposed pipeline of automatic segmentation methods (Fig. 1) consists of three steps: 1. Pre-processing; 2. Seeds Definition; and 3. Segmentation by Geodesic Active Contour.

Image Preprocessing

In the segmentation process, MR imaging artifacts may impair the quantitative delineation of a tissue. To reduce the noise and artifacts, we used pre-processing steps.

Initially, we used the Anisotropic diffusion filter to preprocess image to reduce noise reference. Anisotropic diffusion includes a variable conductance term depends on the differential structure of the image. Thus, the variable conductance can be formulated to limit the smoothing at contours in images, as measured by high gradient magnitude [15]. Previous works have shown anisotropic diffusion offers quantifiable advantages for edge detection in medical images [16].

After anisotropic diffusion filtering, we applied Morphological Gradient and Sigmoidal filters to obtain the image contours. The difference between the dilation and the erosion of an image gives morphological Gradient is useful for edge detection. The sigmoidal filter is widely used as a mechanism for focusing attention on a particular set of values, commonly used as an intensity transform [14].

LV Myocardium Detection

It was necessary to automate LV localization as well to make the whole segmentation procedure automatic. The Hough transform is a widely used technique for detection of geometrical features in images. It is based on mapping the image into a parametric space in which it may be easier to identify if particular geometrical features are present in the image.

A circle Hough transform is used to detect the potential circle approximating the endocardium of the left ventricle [17]. It is based on mapping the image into a parametric space in which it may be easier to identify if particular geometrical features are present in the image. We used The center of circle detected by Hough transform as the origin point of a method that automatically identifies coordinates of seed parameters for Geodesic Active Contour.

Automatic seeds definition

The binary myocardium image defines the myocardial region between epicardium and endocardium. The center of the cavity is represented by 0 (black color), representing a hole in left ventricle short-axis. Seeds should be inserted into the myocardial region. Our method of automatic searching of the myocardium starts in the center of the internal cavity, obtained by Hough Transform. The algorithm runs in four different directions (corresponding the anterior, septal, inferior and lateral segments of myocardium) to find an object of the binarized image, i.e., the endocardial border. We applied morphological filters (fill holes) to eliminate the "holes" referring to the papillary muscles.
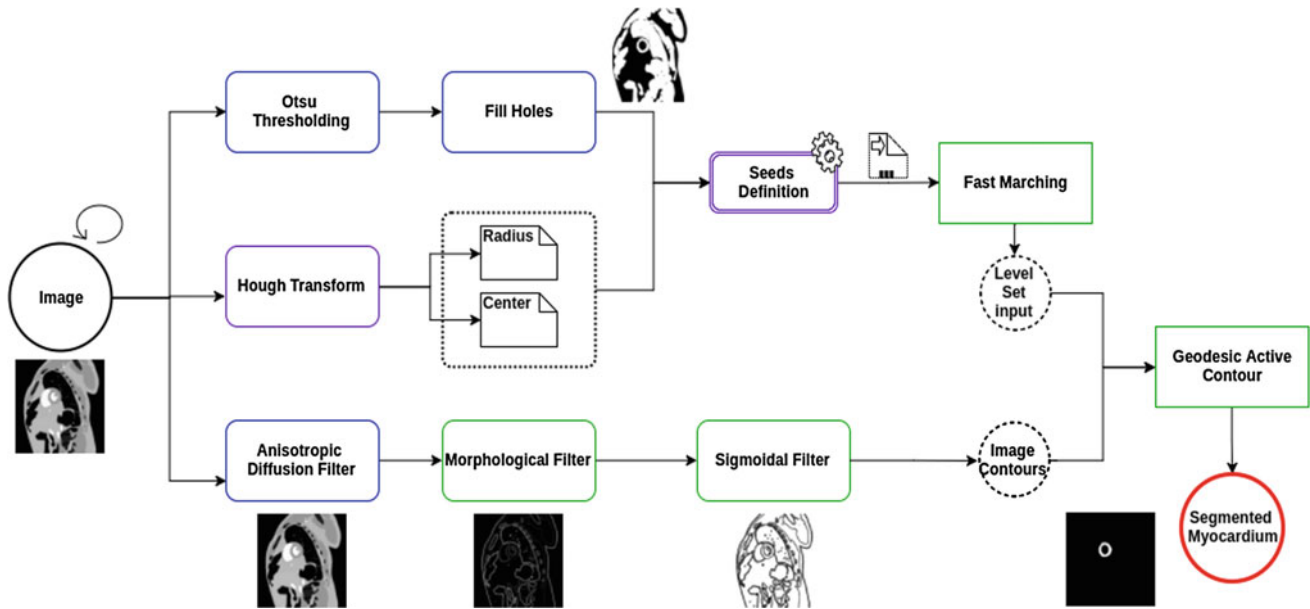
Fig. 1 Automatic myocardial segmentation. The process is divided into 1. Pre-processing (Anisotropic diffusion filter), Morphological filter and sigmoidal filter, 2. Automatic seeds definition (Hough transform, Otsu thresholding, and fill holes), 3. Geodesic active contour

The following procedure then fills the region:

$$X_k = (X_{k-1} \oplus B) \cap A^c, \ k = 1, 2, 3, \ldots$$

where $X_o. = p$, and B is the symmetric structuring element. The algorithm terminates at iteration step k if $X_k = X_{k-1}$. The set union of X_k, and A contains the filled set and its boundary.

Geodesic Active Contour

After the automatic definition of the seeds in the myocardial region, the parameters of the obtained coordinates executed the geodesic active contour.

Snakes or Active contours have often been used for processing of medical images. These deformable models, described by Kass [18], are physically inspired by parametric curves and surfaces, which deform under internal and external forces. The contour is controlled by internal energy, while the external energy forces the contour to move toward the image. The curve of a traditional snake moves through the spatial domain of image to minimize the energy functional [19].

$$E = \int_0^1 \frac{1}{2} \left[\alpha |x'(s)|^2 + \beta |x''(s)|^2 \right] + E_{ext}(x(s)) ds$$

The energy is composed of a first-order term controlled by $\alpha(s)$ and a second-order term controlled by $\beta(s)$. The classical snake approach [18] associates a parametrized planar curve C with an energy

$$E(C) = \alpha \int_0^1 |C'(q)|^2 dq + \beta \int_0^1 |C''(q)|^2 dq$$
$$- \lambda \int_0^1 |\nabla I(C(q))| dq$$

The first two terms control the smoothness (internal energy), while the third term attracts the contour towards the object in the image (external energy). A geodesic curve is a (local) minimal distance path between given points. The following partial differential equation governs the volution of a geodesic active contour [20]:

$$\frac{d\psi}{dt} = -\alpha A(p)\nabla\psi - \beta P(p)|\nabla\psi| + \gamma Z(p)\kappa|\nabla\psi|$$

where A is an advection vector function, P is a propagation (speed) term, and Z is a spatial modifier term for the mean curvature κ. The scalar constants α, β and γ weight the relative influence of each of the terms on the movement of the interface.

2.2 Statistical Analysis and Evaluation

Statistical were performed using Medcalc Statistical Software (version 18.2.1) and R (version 3.2.3).

Experienced imaging cardiologist provided Gold standard annotations of the LV myocardium, i.e., simulated and real

cardiac cine MR. We obtained apical, mid-ventricular and basal segmented slices.

For validation of pipeline segmentation, we use three methods: Dice, Precision and Volumetric Similarity. The automatic segmentation of images is evaluated by comparison with their respective manual segmentation (gold standard) by a cardiologist. Also, for the simulated slices, we evaluated the classic active contour (Snake), using the same seeds obtained by our proposed automatic segmentation method. One can see examples of images along with manual and automatic segmentation in Fig. 2.

The distribution of similarity coefficients obtained by our proposed method and by snake segmentation was displayed in box-and-whisker plots, showing median, first and third quartiles and maximum and minimum. The non-parametric Mann-Whitney test analyzed the differences in the similarity coefficients obtained in simulated images.

3 Results and Discussion

3.1 Simulated Images

Example of images along with manual and automatic segmentation can be seen in Fig. 2. One can see an excellent delineation of epicardial and endocardial borders obtained by our automatic segmentation (GAC) for all levels of signal to noise ratio. These delimitations obtained are visually close to the epicardial and endocardial edges obtained in manual segmentation.

Fig. 2 Definition of the epicardial and endocardial edges obtained in the manual segmentation of the specialist (GS), by the proposed method (GAC) and by the traditional active contour (Snake). Each line represents the result of segmentation in images with different signal to noise ratio. The endocardial and epicardial edges obtained by the classical active contour were undesirable for all levels of signal to noise ratio. For Snake, we used the same seeds obtained by our proposed automatic segmentation method
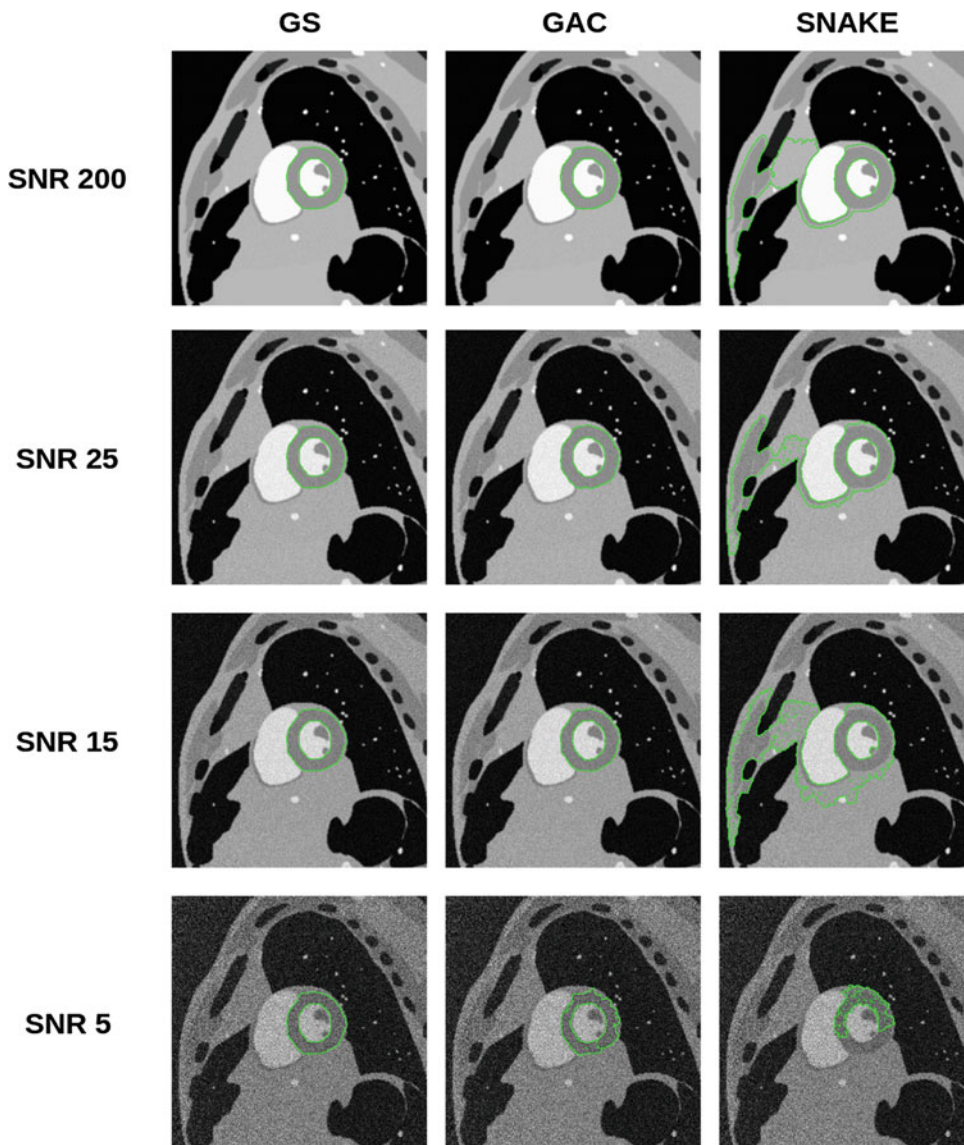
Table 1 Results of the automatic segmentation (Geodesic active contour and snake) compared to manual segmentation using dice, volumetric similarity and precision for different signal to noise ratio. The values express mean values (standard deviations)

	Dice	Vol. similarity	Precision
SNR 200			
Gac	0.98 (0.01)	0.98 (0.01)	0.99 (0)
Snake	0.38 (0.08)	0.40 (0.08)	0.24 (0.06)
SNR 25			
Gac	0.93 (0.04)	0.94 (0.05)	0.98 (0.01)
Snake	0.42 (0.04)	0.43 (0.03)	0.27 (0.03)
SNR 15			
Gac	0.9 (0.06)	0.92 (0.07)	0.97 (0.02)
Snake	0.34 (0.16)	0.35 (0.16)	0.22 (0.13)
SNR 5			
Gac	0.72 (0.16)	0.76 (0.17)	0.82 (0.16)
Snake	0.39 (0.25)	0.54 (0.28)	0.32 (0.27)

Figure 4 and Table 1 shows the comparison of similarity coefficients obtained in simulated images.

Dice show good agreements between manual segmentation and the automatic segmentation (by geodesic active contour) in simulated images with SNR 200, 25, 15 and 5, i.e., 0.98, 0.93, 0.9 and 0.72, respectively. We found moderate agreements between manual segmentation and Snake segmentation in simulated images with SNR 200, 25, 15 and 5, i.e., 0.38, 0.42, 0.34 and 0.39, respectively.

The similarity coefficients Dice and Precision obtained by proposed method were significantly larger than similarity coefficients obtained by Snake in all SNR levels ($p < 0.0001$). The Volumetric Similarity obtained by proposed method was significantly larger than similarity coefficients obtained by Snake in SNR 200, 25 and 15 ($p < 0.0001$) and SNR 5 ($p < 0.01$). The similarity coefficients obtained suggest substantial agreements between the manual and our proposed method segmentation when compared with Snake segmentation.

3.2 Real Images (Chagas Disease)

Figure 3 shows an example of images along with manual and automatic segmentation. One can see a real excellent delineation of epicardial and endocardial borders obtained by our automatic segmentation (GAC) for all consecutive slices (apical, mid-ventricular and basal) obtained by
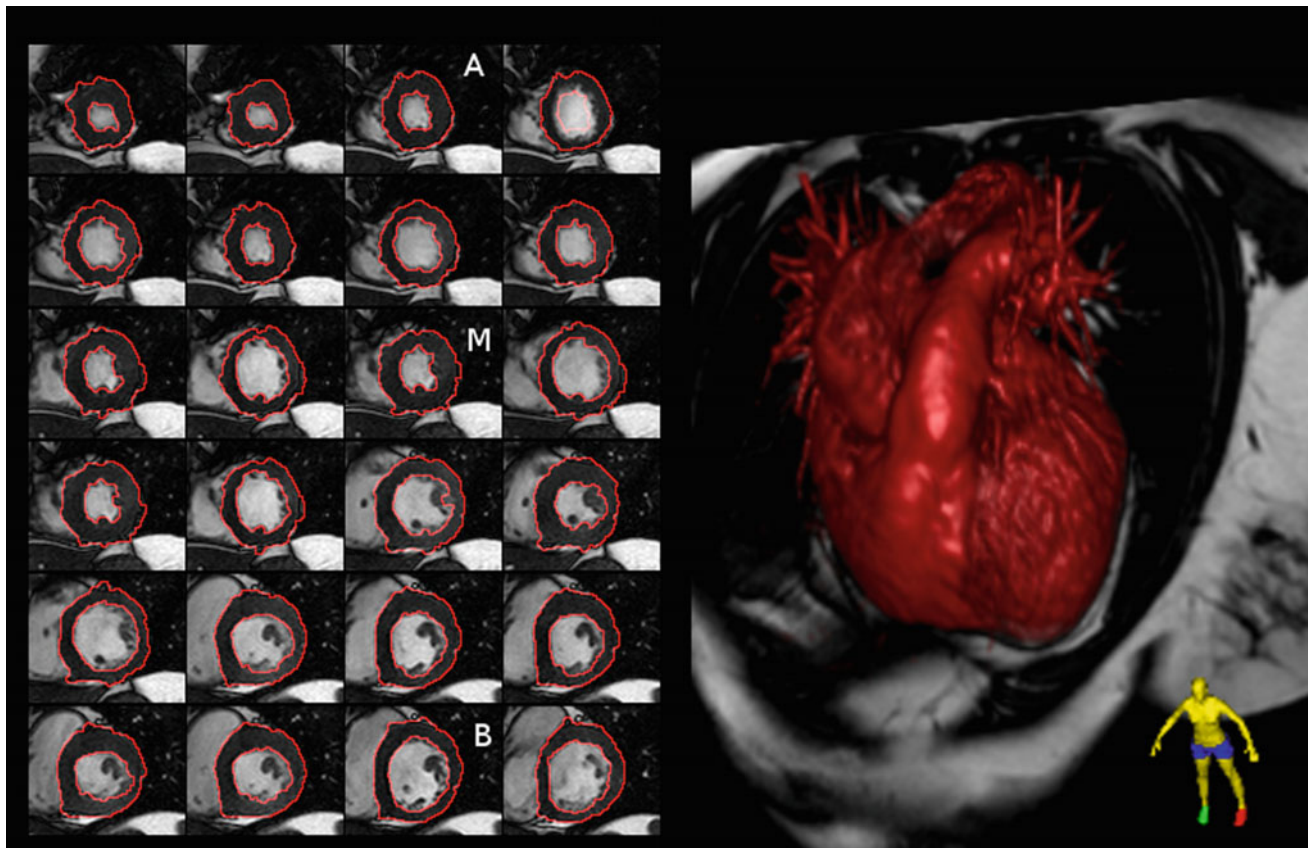

Fig. 3 Delineation of myocardial borders by the proposed method on representative CINE-MR myocardial slices of a patient with the Chagas disease. The figure shows typical apical (A), mid-ventricular (M) and basal (B) slices
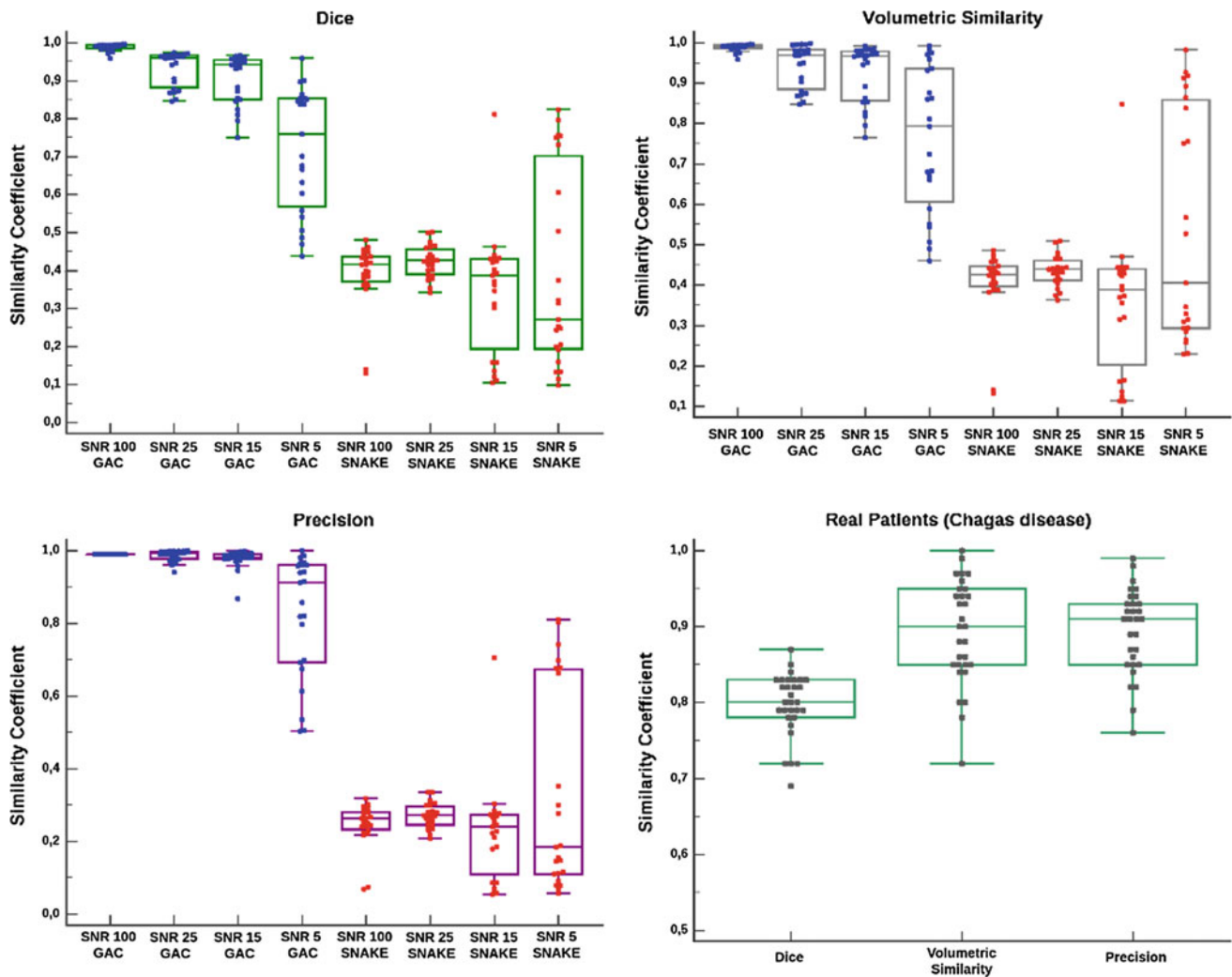
Fig. 4 Comparison of similarity coefficients obtained in simulated and real images. **[Dice; Volumetric Similarity; Precision]**: coefficients obtained by proposed method and snake in simulated images for CINE-MR. These delimitations allow a better assessment of volumes, ejection fraction, and thickening analysis.

different signal to noise ratio. **[Real Patients (Chagas disease)]**: coefficients obtained (Dice, volumetric similarity, and precision) in real images of patients with the Chagas disease

Figure 4 show comparisons of similarity coefficients obtained in real images. The Dice, Volumetric Similarity, and Precision obtained suggest substantial agreements between the manual and our proposed method segmentation in images of Chagas's Disease, i.e., 0.8 [0.69–0.87], 0.89 [0.72–0.99] and 0.9 [0.76–0.98] (mean [min–max]), respectively.

4 Conclusion

Automatic segmentation algorithms are alternative approaches to decrease the time necessary to segment the myocardial area. Our findings suggest that one can use the proposed method in the automatic myocardium segmentation with reliability similar to manual tracing, although entirely free of human interaction. Our proposed method of

fully automatic segmentation provides a better evaluation when compared to solely active contour segmentation. Reliable extraction of measures obtained by automatic myocardium segmentation allows a better assessment of cardiac viability and development of clinical applications.

Conflict of Interest None.

References

1. Tavakoli, V., Amini, A.A.: A survey of shaped-based registration and segmentation techniques for cardiac images. Comput. Vis. Image Underst. **117**(9), 966–989 (2013)
2. Zheng, Q., Lu, Z., Zhang, M., Xu, L., Ma, H., Song, S., et al.: Automatic segmentation of myocardium from black-blood MR images using entropy and local neighborhood information. PLoS One **10**(3), 1–17 (2015)
3. Jolly, M.-P.: Automatic segmentation of the left ventricle in cardiac MR and CT images. Int. J. Comput. Vis. **70**(2), 151–163 (2006)
4. Albà, X., Figueras I Ventura, R.M., Lekadir, K., Tobon-Gomez, C., Hoogendoorn, C., Frangi, A.F.: Automatic cardiac LV segmentation in MRI using modified graph cuts with smoothness and interslice constraints. Magn. Reson. Med. **72**(6), 1775–1784
5. Tsadok, Y., Petrank, Y., Sarvari, S., Edvardsen, T., Adam, D.: Automatic segmentation of cardiac MRI cines validated for long axis views. Comput. Med. Imaging Graph. **37**(7–8), 500–511 (2013)
6. Suinesiaputra, A., Cowan, B.R., Al-Agamy, A.O., Elattar, M.A., Ayache, N., Fahmy, A.S., et al.: A collaborative resource to build consensus for automated left ventricular segmentation of cardiac MR images. Med. Image Anal. **18**(1), 50–62 (2014)
7. Zhu, W., Ha Kang, S., Biros, G.: A geodesic-active-contour-based variational model for short-axis cardiac MR image segmentation. Int. J. Comput. Math. **90**(1), 124–139 (2013)
8. Kurzendorfer, T., Forman, C., Schmidt, M., Tillmanns, C., Maier, A., Brost, A.: Fully automatic segmentation of left ventricular anatomy in 3-D LGE-MRI. Comput. Med. Imaging Graph. **59**, 13–27 (2017)
9. Wang, L., Chitiboi, T., Meine, H., Günther, M., Hahn, H.K.: Principles and methods for automatic and semi-automatic tissue segmentation in MRI data. Magn. Reson. Mater. Phys. Biol. Med. **29**(2), 95–110 (2016)
10. Gho, J.M.I.H., van Es, R., van Slochteren, F.J., Hauer, A.J., van Oorschot, J.W.M., Doevendans, P.A., et al.: A systematic comparison of cardiovascular magnetic resonance and high resolution histological fibrosis quantification in a chronic porcine infarct model. Int. J. Cardiovasc. Imaging **33**(11), 1797–1807 (2017)
11. Folkesson, F.J., Samset, E., Kwong, R.Y., Westin, C.F.: Unifying statistical classification and geodesic active regions for segmentation of cardiac MRI. IEEE Trans. Inf. Technol. Biomed. **12**(3), 328–334 (2008)
12. Wissmann, L., Santelli, C., Segars, W.P., Kozerke, S.: MRXCAT: realistic numerical phantoms for cardiovascular magnetic resonance. J. Cardiovasc. Magn. Reson. **16**(1), 1–11 (2014)
13. Hansen, C.D., Johnson, C.R.: The Visualization Handbook. New York, p. 984 (2004)
14. Johnson, H.J., McCormick, M.M., Ibanez, L.: The ITK Software Guide: Introduction and Development Guidelines version 4.6. Kitware, Inc., p. 248 (2015)
15. Perona, P., Malik, J.: Scale-space and edge detection using anisotropic diffusion. IEEE Trans. Pattern Anal. Mach. Intell. **12**(7), 629–639 (1990)
16. Gerig, G., Kubler, O., Kikinis, R., Jolesz, F.A.: Nonlinear anisotrophic filtering of MRI data. IEEE Trans. Med. Imaging **11**(2), 221–232 (1992)
17. Zhong, L., Zhang, J.M., Zhao, X., Tan, R.S., Wan, M.: Automatic localization of the left ventricle from cardiac cine magnetic resonance imaging: a new spectrum-based computer-aided tool. PLoS One **9**(4) (2014)
18. Kass, M., Witkin, A., Terzopoulos, D.: Active contour models. Int. J. Comput. Vis. 321–331 (1988)
19. Xu, C., Prince, J.L.: Snakes, shapes, and gradient vector flow. IEEE Trans. Image Process. **7**(3), 359–369 (1998)
20. Caselles, V., Kimmel, R., Sapiro, G.: Geodesic active contours. Int. J Comput. Vis. **10**, 1467–1475 (1997)